LIP-STUDENTS-25-07

Application of the Heitler Model to Electromagnetic and Hadronic Showers in Cosmic Ray Simulations

João Cerqueira[1,a], João Vieira[2,b], and Yuri Possidônio[1,c]

[1] *University of Minho, Portugal*
[2] *University of Porto, Portugal*

Project supervisors: Raul Sarmento, Alexandra Fernandes

September 24, 2025

Abstract. In this internship, we were tasked with studying CORSIKA simulations of extensive air showers (EAS), induced by high-energy cosmic rays and configured to match the Pierre Auger Observatory. Using the Heitler model as a simplified framework for describing electromagnetic and hadronic cascades, we evaluate global features of shower evolution — such as the number of particles at shower maximum, the longitudinal development, and the lateral profile. While inherently simplistic, the Heitler model provides valuable insight into the underlying physics of air showers and serves as a pedagogical bridge between analytical theory and full Monte Carlo simulations. This study highlights both the strengths and limitations of such modelling in the context of astroparticle physics.

Keywords: CORSIKA, Extensive Air Showers, Heitler Model, Simulation, ROOT, Cosmic Rays, Muons, Pierre Auger Observatory, Statistical Analysis, Particle Physics, Lateral Distribution, Longitudinal Development

1 Introduction

A little more than a century ago, in 1912, Austrian physicist Victor Hess made a discovery that revolutionized physics and was the jumpstart for the development of the field of particle physics [1]. When physicists were astounded by how a heavily shielded iron chamber would still record traces of radiation, this was thought to be due to the Earth's surface, through which the radiation was being emitted. That's where Hess' discovery comes in: he placed the iron chamber in a hot-air balloon, with a device able to record and register the amount of radiation passing through the chamber. Contrary to what was believed, Hess found out that radiation levels increased with altitude, leading him to conclude that this radiation had an outer space origin [2].

In 1938, in Paris, Pierre Auger and his colleague, Roland Maze, showed that particles separated as far as 20 meters arrived in time coincidence, which meant that these were secondary to a common source. In the Alps, it was shown that this remained true for particles 200 meters apart. One year later, Auger concluded: "One of the consequences of the extension of the energy spectrum of cosmic rays up to 10^{15}eV, is that it is actually impossible to imagine a single process able to give a particle such an energy. [...] the charged particles which constitute the primary cosmic radiation acquire their energy along electric fields of a very great extension.". Even today, there is no clear understanding of which mechanism could give way to such high-energy particles.

The study of cosmic particle showers, its properties and development tries to answer this mysterious riddle and some of the fundamental questions of the field of particle physics. Because these processes occur with such an energy, impossible to reach on Earth with our technology, by studying them we are indirectly probing their origin and getting access to a new physics regime otherwise unreachable. [2]

1.1 The Pierre Auger Observatory

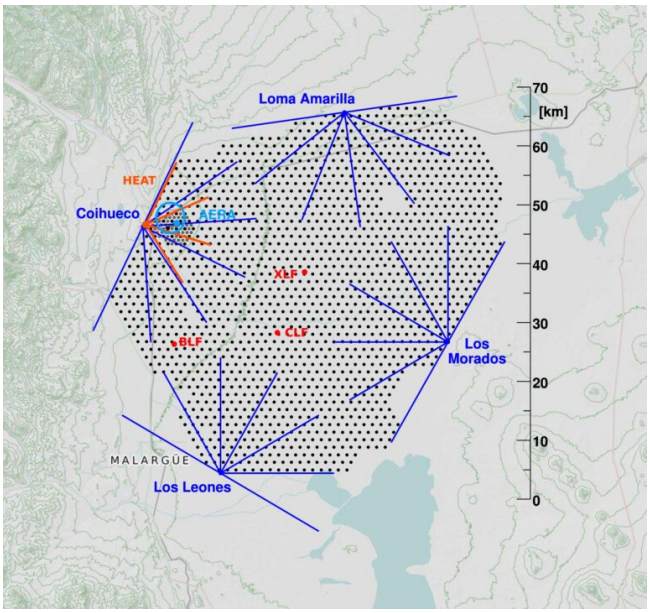

Figure 1: Layout of the observatory[3]

The Observatory's main objective is to study high energy cosmic rays which are not yet understood, as opposed to low energy cosmic rays. One of the challenges the Auger experiment faces is that these showers are very rare: for instance, low energy particle cosmic rays ($\approx 10^{11}$eV) have a

[a] e-mail: joaopmc2004@gmail.com
[b] e-mail: joaovieira476@gmail.com
[c] e-mail: yuri.cals65@gmail.com

flux of 1 particle per m^2s, while for energies above 10^{18}eV it can get as low as 1 particle per km^2year, and even 1 particle per km^2 per century at 10^{20}eV. As rare as they are, they also extend over vast regions.

Because the Observatory has two main detection mechanisms, it is known as a hybrid detector. First, there are surface detectors ranging over an area of 3000km^2, 1.5km apart, responsible for detecting the particles on the ground. Then, the fluorescence detectors track the trail of the nitrogen fluorescence, tracking the development of the air showers by measuring the intensity of the emitted light during the night. While we cannot do anything about the flux of these high energy showers, we can control the area of measurement. The geometry of the Observatory allows the observatory to register approximately one hundred events of energy above $10^{19.5}$eV per year. [4]

2 Heitler Model for Air Showers

What we can actually study are the subproducts of an air shower, after the primary and many more subsequent interactions took place. So, how can we ever study what led to the particles the detectors register? We can break down an air shower into two main observable dependencies: the longitudinal and lateral profiles[5]. The former is a measure of the development of the shower in the atmosphere, as it advances and interacts, forming new particles. Basically, it allows us to know how the number of particles varies with altitude and atmospheric depth. The latter is a measure of how wide the shower spreads at the ground. We take the point of first interaction of the primary and trace its linear trajectory down to the surface. The core of the shower is the intersection of that imaginary line with the Earth.

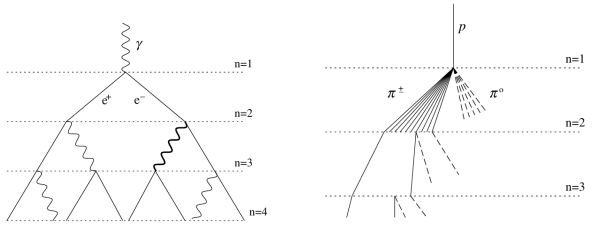

(a) Schematic representation of an electromagnetic cascade, as predicted by Heitler's model.

(b) Schematic representation of a hadronic cascade, as predicted by Heitler's model.

Figure 2: Electromagnetic and hadronic air showers as described by Heitler's model[6].

Now, it is important to understand how the shower develops and what mechanisms are responsible for the particles that we detect. Because they do so in a very complex way, as a combination of electromagnetic and hadronic cascades, Matthews proposes, based on Heitler model, a simplified model that is able to capture the global quantities of these showers, without the complexity of the real world. These global quantities allow us to infer some of the characteristics of the primary particle.

First, we assume the primary to be a single particle, and not a nucleus, for simplicity. The study of nuclei induced showers is a very easy one, after understanding the two simplest models for electromagnetic and hadronic showers [6].

2.1 Electromagnetic showers

For the electromagnetic showers, we take a photon to be the primary. The photon splits into an electron-positron pair (first interaction). After this, both these charged particles undergo a bremsstrahlung process and produce a photon. The processes described repeat themselves with the new particles created, so on and so forth until the individual electron/positron/photon energies drop below the critical energy, ξ_c^e, when the interactions stop. The development of the electromagnetic showers according to Heitler's model are schematically represented in figure 2.

In this simple model, we take the approximation that every particle interacts after travelling a fixed distance across the atmosphere, $d = \lambda_r \ln 2$, called the *splitting lenght*, where λ_r is called the radiation lenght. We denote by n the number of *generations*. The first interaction is then the first generation. According to this model, because for every splitting there are two new particles formed, we have a total $N = 2^n$ number of particles after n generations. It is then obvious that, at the critical energy, where interactions stop, we take n_c splittings to have occured so that the maximum number of particles in the shower is given by:

$$N_{max} = 2^{n_c} \tag{1}$$

Because energy is conserved in the process, we can also take where E_0 is the energy of the primary photon:

$$E_0 = N_{max}\xi_c^e \tag{2}$$

With equations 1 and 2 we get:

$$n_c = \frac{\ln\left(\frac{E_0}{\xi_c^e}\right)}{\ln 2} \tag{3}$$

Finally, another very important physical quantity is X_{max}, which measures the *penetration depth* at which the shower reaches its maximum size. After n splittings it simply is $x = nd$. After n_c generations, where the shower reaches N_{max} we get:[6]

$$X_{max}^{\gamma} = n_c \lambda_r \ln 2 = \lambda_r \ln\left(\frac{E_0}{\xi_c^e}\right) \tag{4}$$

2.2 Hadronic Showers

The hadronic cascades follow a similar concept: a particle undergoing splitting, the products interacting and forming new particles, over and over until they reach a critical energy below which the interactions stop. In this case, we talk about compound particles (hadrons) and so, below the critical energy, there are no interactions but the particles do decay. First of all, let's take a proton to be the primary.

The proton, after striking air molecules, produces pions, both charged and neutral, $\pi^+\pi^-\pi^0$.

Because the π^0 pions are very unstable, they decay quickly into two photons, following the reaction $\pi^0 \rightarrow 2\gamma$, giving way to the development of two EM showers. On the other hand, charged pions interact and produce a new generation of pions, where the behavior of these subsequent particles is the aforementioned. When individual pion energies drop below the critical energy, the interactions stop and the pions decay into muons, $\mu^+\mu^-$ which we observe on the ground and into neutrinos that are not observed. So, the hadronic interactions origin a mixture of a hadronic and electromagnetic (EM) component. As the EM component is dominant, we estimate N_{max} using only that. Taken into account first interaction only we get:

$$N_{max} = \frac{E_0}{3\xi_c^e} \tag{5}$$

Including all the π^0 productions:[1]

$$N_{max} = \frac{E_0}{\xi_c^e}\left(\sum_{i=1}^{n_c}\frac{1}{2}\cdot\left(\frac{2}{3}\right)^i\right) \tag{6}$$

Imagine the atmosphere to be divided into equally thick layers, of thickness $\lambda_I \ln 2$, where λ_I is the *interaction length*. After traversing one layer, hadrons interact and form a new generation of traveling particles. After each interaction, we get both neutral and charged pions, so it is assumed that the number of neutral pions is half the number of charged ones, N_{ch}. We take both λ_I and N_{ch} to be constant, which is a good approximation, but we still need to be cautious of this.

It is easy to conclude that after n generations of interactions, we have $N_\pi = (N_{ch})^n$. If we assume that the energy is equally distributed among every particle, in every generation, we get that the energy per charged pion after n generations is:

$$E_\pi = \frac{E_0}{\left(\frac{3}{2}N_{ch}\right)^n} \tag{7}$$

Using equation 7 we can obtain an expression to calculate n_c:

$$n_c = \frac{\ln\frac{E_0}{\xi_c^\pi}}{\ln\frac{3}{2}N_{ch}} \tag{8}$$

The number of muons in a shower is the same as the number of charged pions at n_c, so $N_\mu = N_\pi = (N_{ch})^{n_c}$, hence:

$$N_\mu = N_\mu^p = \left(\frac{E_0}{\xi_c^\pi}\right)^\beta \tag{9}$$

$$\beta = \frac{ln[N_{ch}]}{ln[\frac{3}{2}N_{ch}]} = 0.85$$

Finally, we can also estimate the maximum shower penetration depth. We will use only the first interaction for this estimation, which will underestimate its value. In the case of hadronic showers, we take into account the hadronic and EM components to obtain:

$$X_{max}^p = \lambda_I \ln 2 + \lambda_r \ln\left(\frac{E_0}{3N_{ch}\xi_c^e}\right) \tag{10}$$

For a nucleus of atomic number A, we simply take the superposition of each individual nucleon. In this case, a nucleus of atomic number A is taken to create A separate proton/neutron air showers with the same starting point. The previous observables are then a product of these multiple air showers, initiated with E_0/A, so we get:

$$N_\mu^A = N_\mu^p A^{0.15} \tag{11}$$

$$X_{max}^A = X_{max}^p - \lambda_r \ln A \tag{12}$$

3 CORSIKA and ROOT

3.1 CORSIKA

CORSIKA is a very powerful tool that helps physicists simulate an air shower. It is a Monte Carlo based program for detailed simulations of extensive air showers initiated by high energy cosmic ray particles.[7]. In this work, we use these detailed simulation results to compare them with Heitler model predictions and to assess the model's validity in estimating the shower's global quantities.

3.2 ROOT

For the treatment, analysis and creation of the graphs of this article, the ROOT software framework was used. ROOT provides efficient handling of large datasets together with powerful statistical and visualization tools.

4 Results and Discussion

Using the information shown in Table 1, we will now study various shower simulations drawing conclusions and testing Heitler's model's validity.

Gamma	
Simulation setup	
Number of showers	1984
Primary energy range	$10^{17.4} - 10^{17.6}$ eV
Incident angle θ	30°
Observables	
Particles per slant depth	Longitudinal profiles; $X_{\max}$ and N_μ dependence on mass
Muons at ground level	Muon distribution
Kinetic energy at ground level	Not used
Distance to shower core	Not used

[1] Check Appendix A for a short but intuitive way to get this expression.

Proton	
Simulation setup	
Number of showers	1, 1000, 3890
Primary energy range	$10^{17} - 10^{17.6}$ eV
Incident angle θ	30°
Observables	
Particles per slant depth	Longitudinal profiles; $X_{\max}$ vs. energy and mass; N_μ vs. mass
Muons at ground level	Muon distribution
Kinetic energy at ground level	Energy spectrum
Distance to shower core	Lateral profile

Helium	
Simulation setup	
Number of showers	1999
Primary energy range	$10^{17.4} - 10^{17.6}$ eV
Incident angle θ	30°
Observables	
Particles per slant depth	Longitudinal profiles; $X_{\max}$ and N_μ dependence on mass
Muons at ground level	Muon distribution
Kinetic energy at ground level	Not used
Distance to shower core	Not used

Nitrogen	
Simulation setup	
Number of showers	1998
Primary energy range	$10^{17.4} - 10^{17.6}$ eV
Incident angle θ	30°
Observables	
Particles per slant depth	Longitudinal profiles; $X_{\max}$ and N_μ dependence on mass
Muons at ground level	Muon distribution
Kinetic energy at ground level	Not used
Distance to shower core	Not used

Iron	
Simulation setup	
Number of showers	1999
Primary energy range	$10^{17.4} - 10^{17.6}$ eV
Incident angle θ	30°
Observables	
Particles per slant depth	Longitudinal profiles; $X_{\max}$ and N_μ dependence on mass
Muons at ground level	Muon distribution
Kinetic energy at ground level	Not used
Distance to shower core	Not used

Table 1: Simulation setup and observables analyzed for each primary particle.

4.1 Single Proton Shower

The first simulation we will study is that of a shower initiated by a primary proton of energy $E_0 = 10^{17}$eV and with an zenithal angle $\theta = 30°$.[2] First, we plot the shower's longitudinal profile to study its development through the atmosphere, as seen in the picture below.

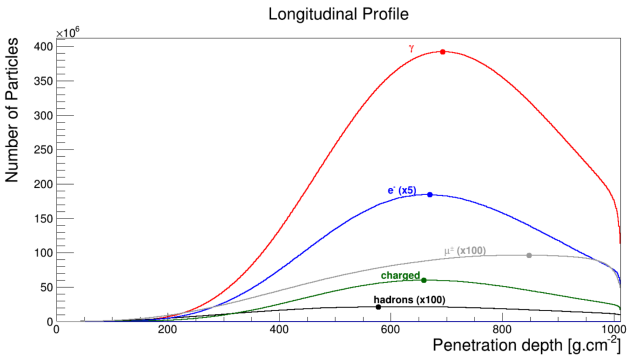

Figure 3: Longitudinal profile of all particles

From this, we can extract the maximum number of photons and electrons observed, each at their respective maximum:

$$N_\gamma^{max} = 3.92424 \times 10^8 \tag{13}$$

$$N_{e^-}^{max} = 1.84885 \times 10^8 (\div 5) \tag{14}$$

This is the first case we observe a "failure" of Heitler's model. The model predicted the number of electrons would surpass photons. The problem lies in the assumption that each electron produces only one photon through bremsstrahlung — whereas in reality, it can produce multiple photons — and that many electrons range out in the air. Simulations confirm that the expected ratio between the number of photons and electrons at their maxima is around 7 [6]. In this case, the ratio is of 10.6. Each particle interacts and decays with a certain probability and the results are directly related to this randomness. Therefore, to obtain more reliable results, we should study averages over many shower simulations.

It's clear that photons and electrons dominate the total number of particles. Muons only appear when charged pions decay, instead of interacting, which is why there's an increase towards higher penetration depths. It would be expected to have no muons before this, but that's not the case. This is because Heitler's model does not take into account that not all pions reach critical energy at the same time, and decays or interactions before that may lead to the production of muons as well.

We now compute the sum of all particles per slant of penetration depth and add the curve to the previous plot (see Fig. 4).

In this case, we cannot know whether the profile represents average behavior or an exception to it. With this in mind, we shall use the results of Heitler's model to make our predictions of N_{max} and X_{max} (see figure 4). Let us start with the simplest part, calculating X_{max}. To do this, we use equation 10. We shall use constant values of $\lambda_I = 120\text{gcm}^{-2}$, $\lambda_r = 37\text{gcm}^{-2}$, $N_{ch} = 10$, $\xi_c^e = 85\text{MV}$, $\xi_c^\pi = 30\text{GeV}$ throughout our discussion, taken from [6].

[2] This is the angle taken between the direction of the ray and vertical axis.

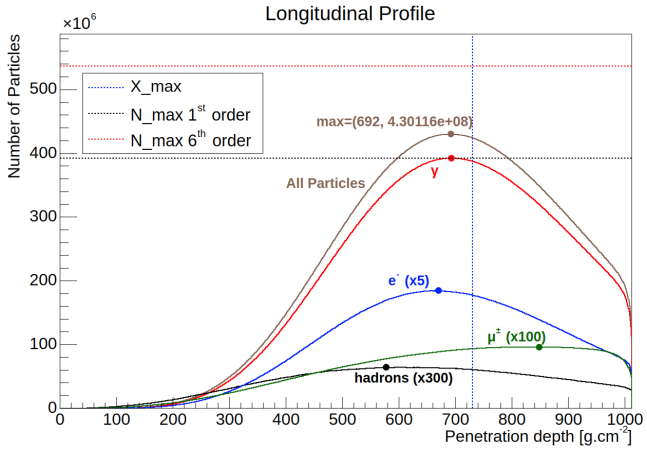

Figure 4: All particles distribution

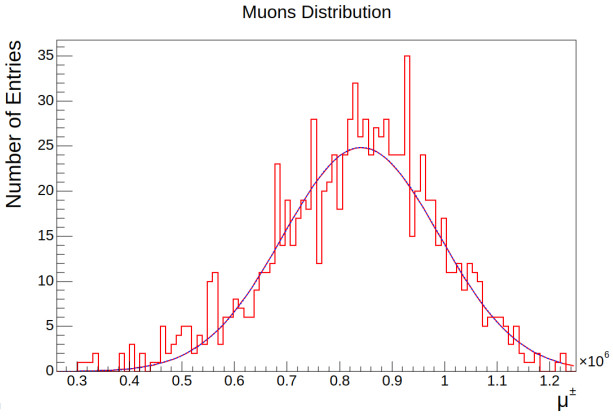

Figure 5: muon number at the ground distribution

So, we obtain a value of $X_{max} = 730.1 \text{gcm}^{-2}$. If we compare with the actual maximum indicated in the figure (692 gcm^{-2}), we obtain an error of 5.22%.

The next value we extract from the plot is $N_{max} = 4.30 \times 10^8$. If we only take the first interaction into account (eq. 5) — a "first order" approximation — it gives a value of 3.92×10^8 and it is already a good estimation. However, how can a model that does not consider particle absorption yield an estimate lower than the simulation result? In fact, we would expect a value twice as high. This discrepancy arises because the model considers only the first interaction.

Including all the terms, i.e until 6th order approximations (eq. 6), we compute a value of $N_{max} = 1.07 \times 10^9$. Notice that this is higher than the simulation result, as expected. Following the model [6], the value is reduced by a factor of two, since absorption effects are not being taken into account, we obtain a more realistic estimate: $N_{max} = 5.37 \times 10^8$. Both estimates are shown in Figure 4.

In this specific case, the error from neglecting higher-order interactions appears to offset the error from neglecting particle absorption.

4.2 One Thousand Proton Showers

In the previous case, we drew conclusions based on one single event. However, the model is intended to describe quantities in terms of average shower behavior. To verify the fluctuations between the showers generated under exactly the same conditions, we plotted the number of muons reaching the ground in each shower, as shown in Fig. 5. The resulting distribution tends towards a Gaussian shape, with some showers exhibiting an average number of muons, while others are comparatively muon-poor or muon-rich.

Selecting three events based on their content — muon-rich, muon-poor, and average — we can plot their corresponding longitudinal (Fig. 6) and lateral profiles (Fig. 8).

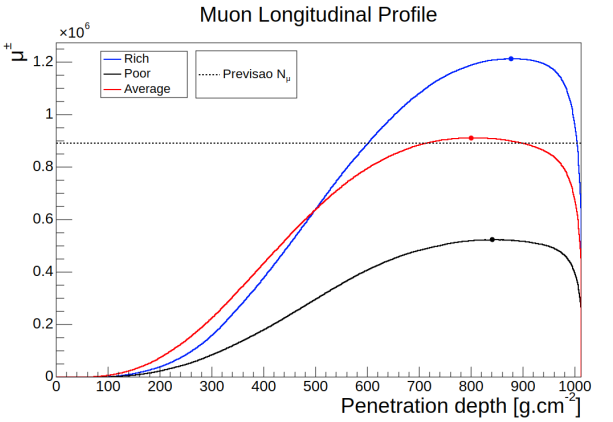

Figure 6: Longitudinal profile of the muon component for 3 events.

From the longitudinal profile and eq.9 we can verify that the model prediction of N_μ fits well with the average shower, as expected.

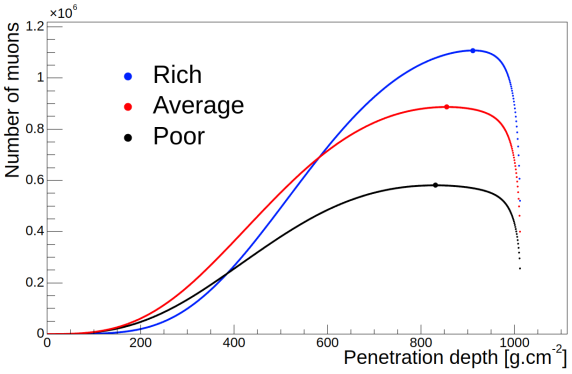

Figure 7: Average Longitudinal Profiles of the muon component for 3 regions of events.

We also observe that the muon-rich shower initially contains fewer muons than the average. This behavior arises because a larger fraction of the primary energy is transferred to charged pions during the first interactions.

As a result, these pions carry more energy and propagate deeper into the atmosphere before decaying, which delays muon production but leads to a stronger muon component later in the shower development. In contrast, for the average case, pions decay earlier, so the number of muons is initially higher but is eventually surpassed by the muon-rich shower.

We can verify this by examining the average profiles for these cases, which demonstrate that the results are not due to statistical fluctuations, as shown in Fig. 7.

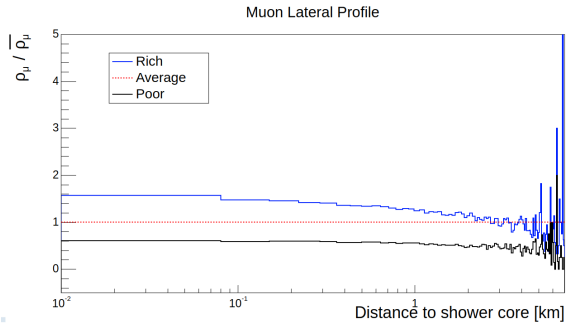

Figure 8: Lateral Profile of the muon component for 2 events relative to average profile

To observe differences between rich and poor relative to the average lateral profile, we computed a ratio histogram by dividing the rich and poor histograms by the average. The result is shown in Fig 8. We observe that the muon-rich profile approaches the average but eventually falls below it, while the muon-poor profile remains approximately at a constant relative distance from the average throughout.

Consistent with the longitudinal profile, muon-rich showers produce muons later (deeper), reducing lateral spread and suppressing the tail at large radius, whereas earlier production in average and muon-poor showers yields broader lateral distributions.

To analyze the energy distribution of muons, referred to as the energy spectrum, we constructed a histogram of the muon energies measured upon reaching the ground (see Fig. 9).

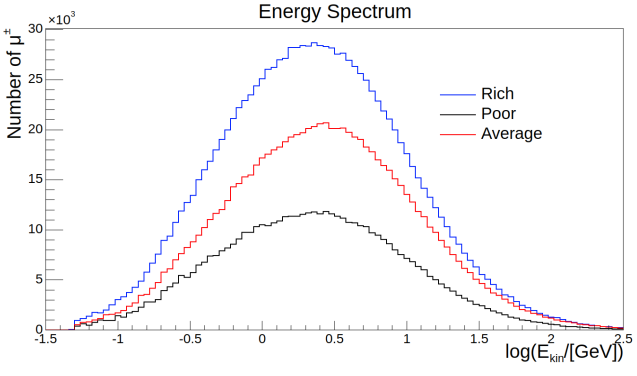

Figure 9: Energy spectrum of the muons at ground of 3 chosen showers

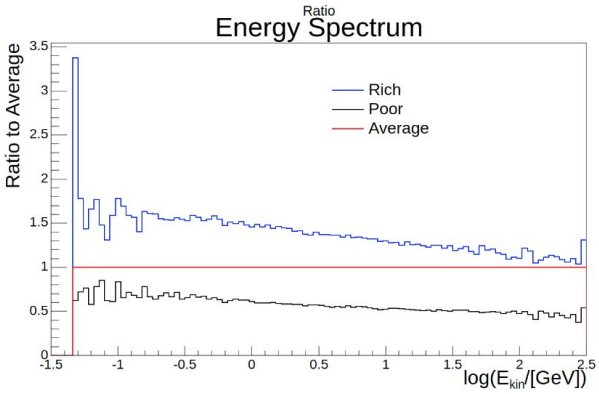

Figure 10: Energy espectrum, relative to average

It can be observed that no muons have energies below $10^{-1.3}$ GeV. This results from a simulation optimization, in which a cutoff energy is introduced to disregard muons below a certain threshold. In this case, the cutoff energy was set to 50 MeV.

From this plot, we can also extract information regarding the higher-energy muons. Muons with energies around $10^{2.5}$ GeV are rare, reflecting the scarcity of muons in the early layers of the shower development. Lower-energy muons are also infrequent. Once again, we can observe the implications of the longitudinal development of muon-rich shower. The muon-poor shower produces fewer muons, in the initial layers, than the average shower, which leads to the production of less high-energetic muons. This explains why, at the end of the spectrum, the distributions of the average and muon-rich showers tend to overlap, while the poor shower remain separated, as shown on Fig. 10.

4.3 Statistical Analysis with Different Primaries

In this section, we begin the statistical study, where it becomes easier to check the compatibility of the model with the overall shower quantities.

Statistical analysis consists of averaging over thousands of events with the same primary characteristics, again at $10^{17.5}$ eV and 30° zenithal angle.

As a first step, we plot the average muon longitudinal profiles for five different primary particles.

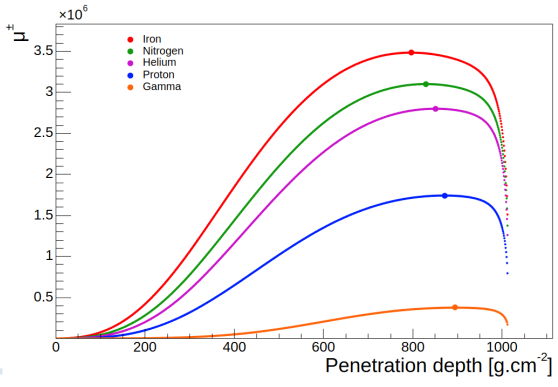

Figure 11: Medium longitudinal profile for muons

We marked with a dot the maximum number of muons reached by each primary in its longitudinal profile. Notice that these maxima are not aligned (see Fig. 11).

In order to study the dependence of this maximum on the primary particle, we plotted it as a function of the primary mass. We then fitted a curve according to the model prediction to check the agreement (see Fig. 12).

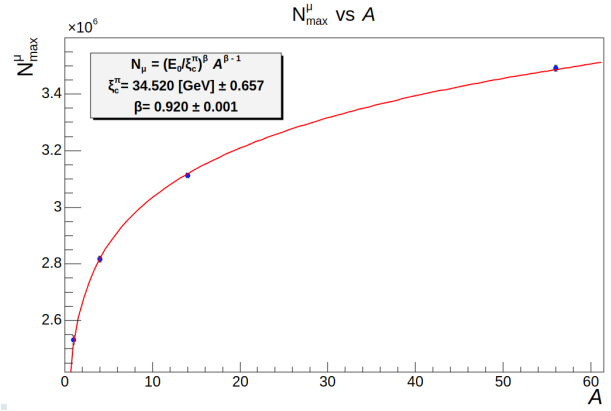

Figure 12: Variation of the number of muons with the atomic mass

The model equation provides a good fit to the points. However, according to the model, the cut-off energy for pions in showers of this energy range should be around 10 GeV, with $\beta \sim 0.85$. Using 30 GeV with $\beta = 0.92$ seems to produce a similar result to using 10 GeV with $\beta = 0.85$, since in Fig. 6 the model parameters fit well on average, for proton. Changing β primarily affects the multiplicity of charged pions ($\beta = 0.92 \rightarrow N_{\rm ch} \sim 50$), whereas changing the cut-off energy modifies the layer where the shower reaches its maximum. Thus, these two parameters are directly related to the depth at which the pions penetrate the atmosphere.

Afterward, we compute a similar plot, but now not only for muons, but for all components. According to the model equation, the dependence of $X_{\rm max}$ on the atomic mass A is expected to follow a logarithmic behavior.

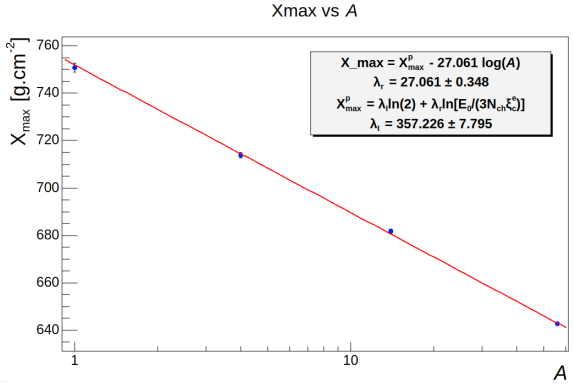

Figure 13: Variation of X_{max} with the atomic mass

Since the x-axis is in logarithmic scale and the curve fits a straight line, we can conclude that the model predicts well the logarithmic dependence of $X_{\rm max}$ on the primary mass. However, the parameters used in the model fall outside the acceptable ranges when compared with the fitted curve, taking into account the errors associated with the average calculations.

Since we already see the variation of $X_{\rm max}$ with the number of mass, the only remaining plot (with respect to the $X_{\rm max}$) is the one illustrating the behavior of $X_{\rm max}$ as a function of the primary energy. To this end, we analyzed a sample of 3890 proton-induced showers with energies ranging from 10^{17} to $10^{17.6}$ eV. The energies were divided into bins of width 0.1 in the logarithm of the primary energy, and for each bin a histogram was constructed in order to extract both the average value of $X_{\rm max}$ and the associated statistical uncertainty. The resulting plot is presented in Figure 14.

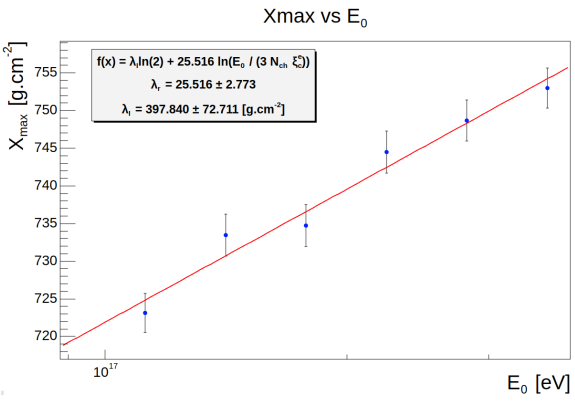

Figure 14: Variation of X_{max} with the primary energy

The Heitler model predicts a logarithmic dependence of $X_{\rm max}$ on the primary energy, which is consistent with our results, as the fitted straight line intersects all error bars. The model further predicts a value of $\lambda_I \ln 2 = 83.18$ g/cm^2, while our analysis yields 275.76 ± 50.40 g/cm^2. Since the model accounts only the first-order interaction, a systematically larger value——at least 100 g/cm^2 [6]—was expected .

To finalize, we computed the number of muon distributions for all primaries analyzed (see Fig.15). We observed the regions where the distribution of each primary is concentrated, noting in some cases the data show a larger spread. For instance, in photon-induced showers, which usually contain very little hadronic component, there is an event that reached a muon count comparable to the iron average. For photon initiated showers we can have a purely electromagnetic shower consisting only of electromagnetic radiation ($e^\pm$ and γ), arising from processes such as $\gamma \rightarrow e^+e^-$ and $e^\pm \rightarrow e^\pm\gamma$, and can therefore theoretically produce zero muons. However, if the photon undergoes a hadronic interaction in the first collisions, secondary hadrons can be generated, which may result in a muon content. For heavy primaries, such low-muon scenarios are not possible, and the muon production remains consistently higher.

For heavier primary nuclei, the average number of muons in extensive air showers is larger. This follows from the superposition principle, since a nucleus of mass number A can be seen as A nucleons, each initiating a subshower.

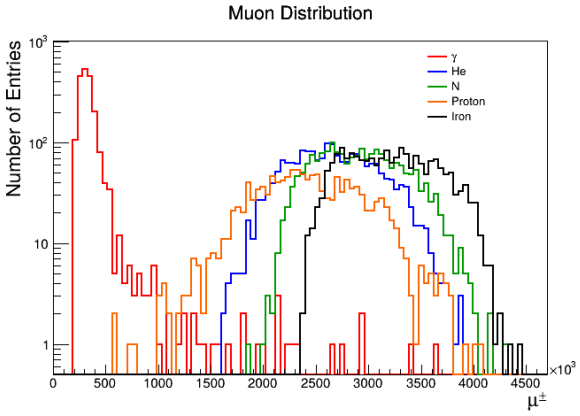

Figure 15: Distribution of the number of muons at ground for different primaries

5 Conclusion

Through the study of simulated air showers, we were able to systematically study its components while probing Heitler's model's validity. Our results showed us that this very simplistic picture can make valid physical predictions for important shower quantities, such as the maximum penetration depth and the number of particles. Even when our results were not directly explained by Heitler's model, the basic assumptions that we made could be easily replaced by better, more complex ones which allowed us to explain some unexpected results - such as a photon induced shower having a muon component; see, for example, figures 11 or 15. We use the model as a basis for our work, but are aware of the fact that real-life randomness is not taken into consideration and helps us explain some of our results. Heitler's model idealizes a shower, where every particle has the same evolution throughout the shower. This is simply not what actually happens. From our results, we can be confident that Heitler's model is valid (under the right assumptions) and correctly depicts shower behavior and captures all of the basic physics needed to understand them.

6 Acknowledgements

We thank LIP for the opportunity to participate in this project, allowing us to improve our programming skills in C++ and data analysis with ROOT, as well as learning about extensive air showers, the physical processes behind cosmic ray interactions, and the importance of this in the field of Particle Physics.

References

[1] C. Grupen, *Astroparticle Physics* (Springer, 2005), chap. 1.1

[2] J.W. Cronin, Rev. Mod. Phys. **71**, S165 (1999)

[3] The Pierre Auger Collaboration, *The pierre auger observatory* (2024), `https://pages.lip.pt/auger/the-pierre-auger-observatory/`

[4] The Pierre Auger Collaboration, *The pierre auger observatory* (2024), `https://www.auger.org/observatory/observatory`

[5] R. Sarmento, internal presentation, LIP Minho (June 2025)

[6] J. Matthews, Astroparticle Physics **22**, 387 (2005)

[7] D. Heck, T. Hüge, T. Pierog, *Extensive Air Shower Simulation with CORSIKA: A User's Guide*, Institut für Astroteilchenphysik, Karlsruhe, Germany (2025)

A Appendix

We need to keep in mind that the total number of particles is strongly dominated by the number of photons/electrons, or simply the total number of particles in an EM shower, given by equation 1. Another important thing to remember is the neutral pion decay $\pi^0 \to 2\gamma$, giving way to two EM subshowers. Each of these subshowers will have a primary energy equal to half the energy of the pion that originated it, $E_\pi = \frac{E_0}{\frac{3}{2}N_ch}$, as in equation 7, so that $E_\gamma = \frac{1}{2}E_\pi$. In this way, using this result, we get, for one pion:

$$N^{\pi^0}_{max} = 2 \times \frac{E^\gamma_0}{\xi^e_c} \tag{15}$$

To estimate over all pions:

$$N_{max} = N_{\pi^0} N^{\pi^0}_{max} = 2 \times N_{\pi^0} \frac{E^\gamma_0}{\left(\frac{3}{2}N_{ch}\right)\xi^e_c} \tag{16}$$

It can easily be shown that for the n-th generation the result is simply:

$$N^n_{max} = 2 \times N_{\pi^0} \frac{E^\gamma_0}{\left(\frac{3}{2}N_{ch}\right)^n \xi^e_c} \tag{17}$$

Because $N_{ch} = \frac{1}{2}N_{\pi^0}$, the above equation can be easily rewritten in a simpler form, as 6:

$$N_{max} = \frac{E_0}{\xi^e_c}\left(\sum_{i=1}^{n_c} \frac{1}{2} \cdot \left(\frac{2}{3}\right)^i\right) \tag{18}$$